

RAVEN, a New Software for Dynamic Risk Analysis

C. Rabiti^a, A. Alfonsi^a, J. Cogliati^a, D. Mandelli^a, R. Kinoshita^a

^a Idaho National Laboratory, Idaho Falls, USA

Abstract: RAVEN (Risk Analysis Virtual Environment) is a generic software driver to perform parametric and probabilistic analysis of code simulating complex systems. Initially developed to provide dynamic risk analysis capabilities to the RELAP-7 code, [1] RAVEN capabilities are currently being extended by adding Application Programming Interfaces (APIs). These interfaces are used to allow RAVEN to interface with any code as long as all the parameters that need to be perturbed are accessible by inputs files or directly via python interfaces. RAVEN is capable to investigate the system response, probing the input space using Monte Carlo, grid strategies, or Latin Hyper Cube schemes, but its strength is its focus toward system feature discovery, such as limit surfaces, separating regions of the input space leading to system failure, using dynamic supervised learning techniques. The paper will present an overview of the software capabilities and their implementation schemes followed by some application examples.

Keywords: PRA, Limit Surface, Reliability.

1. INTRODUCTION

1.1. Project Background

The RAVEN [2-4] project was started at the beginning of 2012 to provide a modern framework for risk evaluation for Nuclear Power Plant (NPPs). RAVEN, under the support of the Nuclear Energy Advanced Modelling and Simulation (NEAMS) program, has been tasked to provide the necessary software and algorithmic tools to enable the application of the conceptual framework developed by the Risk Informed Safety Margin Characterization (RISMC) path-lead [5]. RISMC is one of the paths defined under the Light Water Reactor Sustainability (LWRS) DOE program. In its initial stage of development RAVEN has focused and optimized for the RELAP-7 code, currently under development at Idaho National Laboratory as future replacement of the RELAP5-3D [6] code. Since most of the capabilities developed under the RAVEN project for RELAP-7 are easily deployable to other software, currently side activities are on going for coupling RAVEN with other codes such as RELAP5-3D and BISON (fuel performance code) [7]. This paper focuses on the description of the software infrastructure and the current capabilities that are available to any generic code.

1.2. Software Goals

Before starting a more deep exploration of the software capabilities and their implementations it would be helpful to review in more detail the tasks that the project was designed to accomplish. RAVEN is essentially designed as a discovery environment to characterize system responses and, in particular, to compute the risk connected to the operation of a particular system. Risk is obviously defined following the engineering approach by:

$$R = \int_X \int_{t_0}^{t_{end}} C(\bar{x}, t) pdf(\bar{x}, t) dt d\bar{x}.$$

Where:

- \bar{x} : vector of the system coordinates in the phase space
- t : time
- t_0 : initial time
- $pdf(\bar{x}, t) dt d\bar{x}$: probability of the system being in $d\bar{x}$, centred in \bar{x} , at a time within dt , centred in t
- X : support of $pdf(\bar{x}, t)$
- $C(\bar{x}, t)$: cost function

The analysis of risk, defined above, is meaningful for systems for which it is not possible to build a fully deterministic representation and here referred as dynamic stochastic systems. Unfortunately, these represent most of the systems of practical interest in engineering. The stochastic behaviours, or impossibility of defining a fully deterministic model, is imposed by uncertainties in the initial conditions, in the parameters characterizing the mathematical models used to simulate the system and by intrinsically stochastic laws, characterizing the underlining physics.

Given that, an analysis code such as RAVEN aims to investigate the probability of the system to be located within a certain region of the phase space. This is a classical task that could be accomplished, for example, using the Monte Carlo (MC) method. MC is, unfortunately, notoriously computationally expensive and therefore other sampling strategies have been and will be implemented in RAVEN.

While the evaluation of the risk is per se a relevant task, it is even more important to map the behaviour of the risk as a function of the initial condition and of the parameters characterizing the system behaviour (input space). The knowledge of the relationship among risk, initial conditions and model parameters guides engineers improving the systems, prioritize additional experiments to reduce uncertainty on selected parameters, and the development of more accurate models. RAVEN uses its sampling methodologies to support the engineer in investigating such relationships, in a fast and focused fashion.

2. THE SOFTWARE

2.1 The Basic Elements

RAVEN is coded in Python and has a highly object oriented design. The framework can be described through few (not all) key basic objects. A list of these objects and a brief description is reported here while they will be explained more in detail in the following paragraphs:

- *Distribution*: In order to produce realization of the input parameters and initial conditions, RAVEN requires the capability to sample the possible values, based on their probabilistic distribution. In this respect, a large library of probability distribution functions is available.
- *Sampler*: A proper strategy to sample the input space is fundamental to the optimization of the computational time. A sampler, in the RAVEN framework, connects a set of variables to their corresponding distributions and produces a sequence of points in the input space.
- *Model*: A model owns the representation of the physical system; it is therefore capable to predict the (or one of the possible) evolution of the system given a coordinate set in the input space.
- *Surrogate Models (SM)*: As already mentioned the construction of the risk variation, as a function of the coordinates in the input space, is a very expensive process, especially when brute force approaches, i.e. Monte Carlo methods, are used. Surrogate models are used to speed up this process by reducing the number of needed points and prioritizing the area of the input space to be explored.

In addition to the ones already mentioned, there are others important entities (objects) in the RAVEN framework but they are more closely related to the software infrastructure and therefore less important in the illustration of the analysis capabilities of the RAVEN code.

2.2. Distribution

As already mentioned, the capability to properly represent variability in the input space is tied into the availability of the proper probabilistic distributions. RAVEN implements an interface to the Boost library [8] that makes available the following univariate distributions: Bernoulli, Binomial, Exponential, Logistic, Lognormal, Normal, Poisson, Triangular, Uniform, Weibull, Gamma, and Beta. All distributions are also available in their truncated form when this is mathematically feasible. Figure 1 shows a scattered plot of a Lognormal, normal and uniform distributions (with their respective equations) obtained with an equally probable spaced grid with respect to the sampled parameters.

Many times, parameters that need to be sampled are subject to correlations. This is the case, for example, when the same experimental setting is used to measure more physical parameters that are then incorporated in the mathematical models. In this case it is possible that experimentalist might suggest that the error on those parameters is correlated by, for example, a common type of dispersion. In case of any two of the stochastic variables affecting the system correlated variables correlated

variables (\mathbf{p}_i and \mathbf{p}_j) it is not possible to determine the probability that $\mathbf{p}_i = \bar{\mathbf{p}}_i$ without knowing the value of \mathbf{p}_j . Another common situation that leads to correlate variables is when the probability of failure of a particular component is derived from databases collected with multi dimensional parameterization; for example, number of load cycles and average environmental temperature to which the component is exposed. Currently in RAVEN it is possible to describe both N-dimensional (i.e., multivariate) Cumulative Distribution Functions (CDF) and Probability Distribution Functions (PDF) by means of external files that provide the probability (or cumulative probability) values as a function of the interested parameters. The grid at which the probability/cumulative probability is provided could be Cartesian (possibly non regular) or completely sparse. The available algorithms to interpolate the imported CDF/PDF are n-dimensional splines [9] (only Cartesian grid) and inverse weight [10]. Internally, RAVEN provides also the needed n-dimensional differentiation to derive from the CDF the PDF and eventually the integration to derive the CDF from the PDF.

$$\begin{aligned} &Normal(x; \sigma = 0.5, \mu = 0) \\ &= N(x; \sigma = 0.5, \mu = 0) = \frac{1}{\sigma\sqrt{2\pi}} e^{-\frac{(x-\mu)^2}{2\sigma^2}}, \end{aligned}$$

$$\begin{aligned} &Lognormal(x; \sigma = 0.5, \mu = 0) \\ &= LN(x; \sigma = 0.6, \mu = 0) \\ &= \frac{1}{x\sigma\sqrt{2\pi}} e^{-\frac{(\ln(x)-\mu)^2}{2\sigma^2}}, \end{aligned}$$

$$\begin{aligned} &Uniform(x; min = 0, max = 3) \\ &= U(x; min = 0, max = 3) \\ &= \frac{[H(x) - H(3 - x)]}{3} \end{aligned}$$

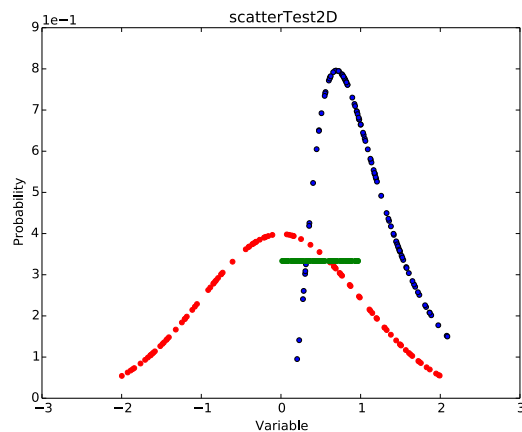


Figure 1: Scattered plot generated by sampling (Latin Hypercube sampling scheme) of a Normal (red), Lognormal (blue) and Uniform distributions (green).

One of the biggest challenges in using multidimensional distributions is lack of an inverse. When, for example, a Monte Carlo sampling strategy is used for univariate distributions, first a random number between 0-1 is generated, then the CDF at that point is inverted to get the value of the variable to be used in the simulation. The existence of the inverse of the CDF is guaranteed in the univariate case by the monotonicity of the CDF. In the N-Dimensional case this is not sufficient since the CDF is a function $CDF(\mathbf{A} \subseteq \mathbf{R}^N) \rightarrow [0, 1]$ and therefore could not be a bijection. This situation is illustrated in figure 2 where the failure probability of a pipe is provided as function of the temperature and the pressure. The plane identifies an iso-probability line (in general an iso-surface) along which all points (pipe temperature and pressure) satisfy the 0.5 value of the CDF. When multivariate distributions are used RAVEN implements a surface finding algorithm to identify the location of the iso-surface and then chooses randomly a point on this surface. A similar strategy is also used when, like in the Latin Hypercube Sampling (LHS), the points are required to be within a certain CDF band.

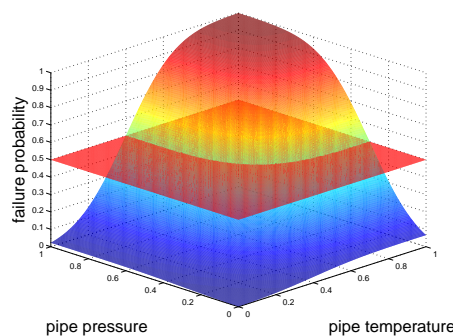


Figure 2: Demonstrative multivariate CDF of the failure of a pipe as a function of temperature and pressure.

2.3. Sampler

The samplers are one of the most developed part of the RAVEN framework and the ones that will receive also more attention in the future given its crucial importance in increasing the effectiveness of the computational resources. There are three main classes of samplers: blind samplers, dynamic event tree samplers, and adaptive samplers. Given the extension of the argument and its importance each type will be treated separately.

2.3.1 Blind Sampler

Under the name of blind sampler we collect the samplers that neither take advantage of the information collected by the already performed sampling of the system (adaptive samplers) neither take advantage of common patterns that different sampling might generate in the phase space (dynamic event trees).

They belong to this type of samplers and are implemented in RAVEN, Monte Carlo, Cartesian grids, and Latin Hypercube. To illustrate the different features of the samplers we can compare figures 3 to 5. On the left side all the figures have the reconstruction of the distributions used (the ones also referred in figure 1) in the center the sampling point dispersion in the 3D space and on the right the reconstruction of the N-Dimensional probability (the variable distributed following the uniform distribution has been suppressed since it only provides a scaling factor).

The sampler type and parameters used for the different figure are the following:

- Figure 3: Grid sampler, 21 points over the Lognormal and Normal distribution equally spaced in cumulative probability, 4 points over the uniform distribution equally spaced in variable values. Total number of sampling 1764.
- Figure 4: Monte Carlo sampling, 300 total sampling.
- Figure 5: LHS sampling, 100 total sampling equally spaced in cumulative probability.

From the comparison of the 3 figures it is evident how the LHS (figure 5), which is nowadays probably the most used of the blind samplers, provides a good coverage of each single distribution (2D plot on the right) but still results in a very sparse scatter plot of the sampling location in the 3D (center) scatter plot. Clearly the grid-based sampler is the one that has discovered the most of the underlining probabilistic structure (figure 3 on the right) but it is also the most expensive. All these samplers are well know, as well as their properties, therefore it is not of interest to further investigate their application.

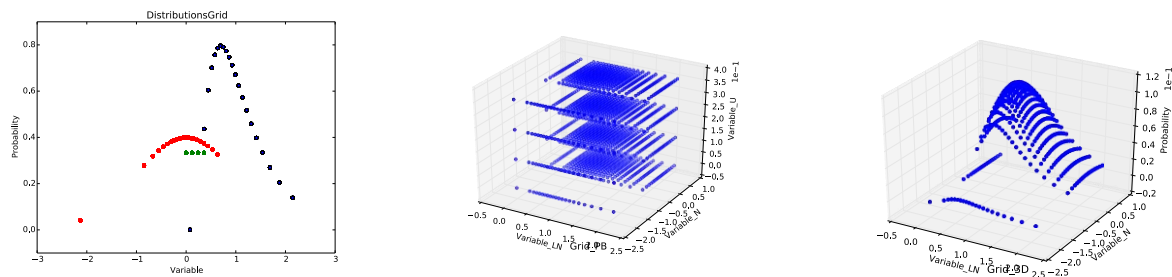


Figure 3: Grid based sampler. From the left: sampling point on the distribution, 3D dispersion of the sampling point coordinate, and probability map.

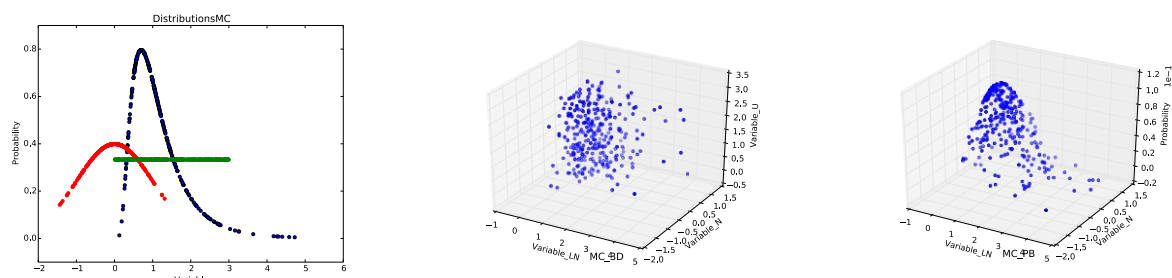


Figure 4: Monte Carlo sampling. From the left: sampling point on the distribution, 3D dispersion of the sampling point coordinate, and probability map.

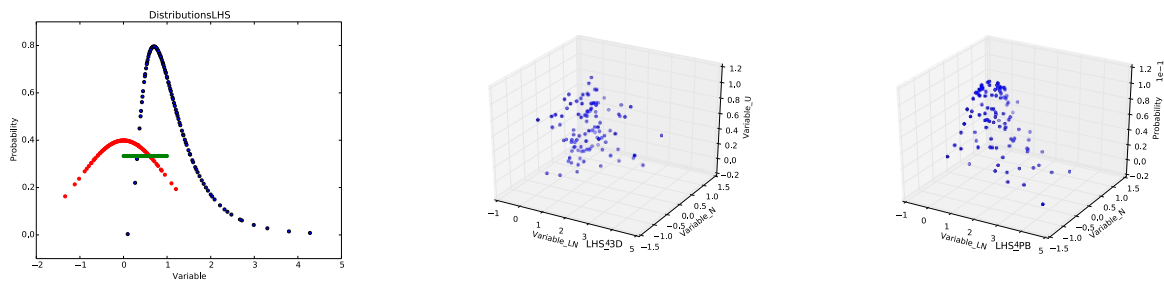


Figure 5: LHS based sampler Grid based sampler. From the left: sampling point on the distribution, 3D dispersion of the sampling point coordinate, and probability map.

2.3.2 Dynamic Event Tree Sampler

The main idea that has led to the success of the dynamic event tree approach [11] is the consideration that some events, characterizing the stochastic behavior of the system, might influence the trajectory in the phase space only from a certain point in time onward. Given this consideration, it is natural to seek a way to leverage this to reduce the computational burden.

Similarly to a grid based sampling approach, a N-Dimensional grid is built on the CDF space. A single simulation is started and a set of triggers are added to the control logic of system code so that at each time, one of the CDF point in the grid is exceed (this is determined by monitoring the evolution of the system in the phase space) a new simulation is started. The probability associated to each simulation is partitioned so that the branch where the exceeding of the CDF leads to a transition in the phase space carry a fraction equal to the CDF exceeded threshold and the one where nothing happens it carries the complementary probability.

Figure 6 shows a practical example. We assume that the probability failure of a pipe is proportional to the pressure inside (on the top right), and a three intervals grid is applied on the CDF. One simulation is started (0) and, when the control logic after a certain amount of time detects reaching 33% of the CDF, stop the simulation and start two new branches. The restarted simulation with the broken pipe (red line) carries 33% of the probability while the other with the pipe still intact carries 66% of the probability. The same procedure is repeated at point 2.

Of course not all parameters could be sampled using a dynamic event tree approach, generally it is common practice to sample the parameters affected by aleatory (statistical) uncertainty using the event tree approach and sampling the input space for the ones subject to epistemic uncertainty. In reality the determination of the possibility/impossibility to sample a variable in one of the two ways is more complex and ties into the possibility to construct a phase space such as the evolution of the probability density function for the system could be represented by the Liouville equation. A more detailed discussion on this issue could be found in [3]. For example it would be possible to add to the input space the failure pressure of the pipe and this would allow performing a Monte Carlo preserving the probabilistic structure of the system. On the other side if the friction coefficient inside the pipe is considered as an uncertain parameter, this would lead to an immediate branching of the simulation making the dynamic event tree approach just a grid sampling on the input space. There are also cases where the aleatory variables could not be casted into initial condition but, even if at a costly expansion of the phase space, this is possible in most of the cases of practical interest. At the moment a hybrid approach (sampling of initial condition plus dynamic event trees) is not yet implemented but it is foreseen being available in the next months.

As already mentioned, the dynamic event tree requires an interaction between the software performing the simulation of the physical system and a control logic capable to evaluate what is the CDF value for the current system coordinate in the phase space, and eventually stopping the simulation. Not all codes possess this capability and even if available it should be accessible by RAVEN code so to modify the CDF thresholds according to the branching pattern. Currently this capability is fully available for RELAP-7 and being tested for RELAP-5.

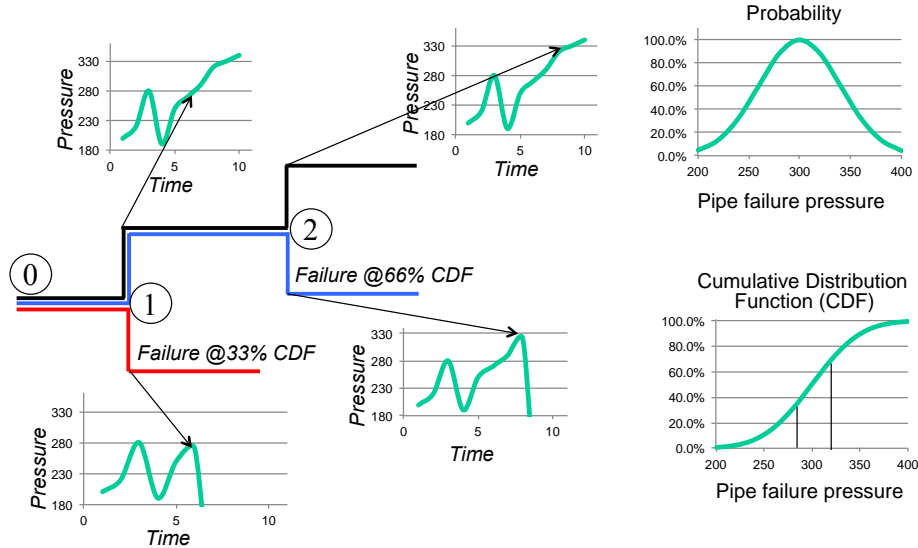


Figure 5: Dynamic Event Tree simulation pattern.

2.3.3 Adaptive samplers

One of the more advanced options that RAVEN offers is goal oriented sampling strategies for the research of limit surfaces. To properly explain which type of information is available by these techniques it is useful to start from the characterization of limit surfaces in system where the probabilistic behavior is generated only as a function of uncertainty in the model parameters (\bar{p}) and initial condition \bar{x}_0 only.

In such a cases:

$$\int_{\bar{X}} \int_{t_0}^{t_{end}} pdf(\bar{x}, t) dt d\bar{x} = \int_{t_0}^{t_{end}} \int_{\mathcal{P}} \int_{X_0(\bar{p}, t)} pdf(\bar{x}_0, \bar{p}) d\bar{x}_0 d\bar{p} dt.$$

Where:

$\bar{p} \in \mathcal{P}$: space of the variability of the parameters characterizing the model

$X_0(\bar{p}, t) = \{\bar{x}_0 | H(\bar{x}_0, \bar{p}, t) = \bar{x}\}$: space of the variability of the initial condition that for a given set of parameters brings the system at the coordinate \bar{x} at time t along the $H(\bar{x}_0, \bar{p}, t)$ mapping (being $H(\bar{x}_0, \bar{p}, t)$ the transfer function of the system).

For convenience it is possible to remove the distinction between uncertain parameters and uncertain boundary condition by introducing $\bar{r}(t) = (\bar{x}_0, \bar{p})(t) \in \mathcal{S}$ where

$$\mathcal{S}(t) = \{(\bar{x}_0, \bar{p}) | H(\bar{x}_0, \bar{p}, t) = \bar{x}\}.$$

As a consequence:

$$\int_{\bar{X}} \int_{t_0}^{t_{end}} pdf(\bar{x}, t) dt d\bar{x} = \int_{t_0}^{t_{end}} \int_{\mathcal{S}(t)} pdf(\bar{x}_0, \bar{p}) d\bar{r} dt.$$

In many engineering cases the cost function is just a Heaviside function describing the availability of the system (1 system available, 0 system down). In a generalized description it is more appropriate to use the characteristic function of the failure domain θ_f that for simplicity is assumed to depend only on the status of the system at the end of the simulation time (mission time) since this does not alter the conclusion hereafter derived.

$$\theta_f(\bar{x}, t_{end}) = \begin{cases} 0 & \text{if } \bar{x} \in X \setminus X_f \\ \delta(t - t_{end}) & \text{if } \bar{x} \in X_f \end{cases}$$

Where X_f is the region of the phase space where the system is not available.

By replacing this definition of the cost function, the integral that define the risk becomes:

$$R = \int_{\bar{X}} \int_{t_0}^{t_{end}} \theta_f(\bar{x}) pdf(\bar{x}, t) dt d\bar{x} = \int_{X_f} \int_{t_0}^{t_{end}} \delta(t - t_{end}) pdf(\bar{x}, t) dt d\bar{x} = \int_{X_f} pdf(\bar{x}, t_{end}) d\bar{x}.$$

Now by expressing the probability density function of the system by the probability density function of the initial condition and uncertain parameters

$$R = \int_{S_{end}} pdf(\bar{x}_0, \bar{p}) d\bar{r},$$

where $S_{end} = S(t_{end})$.

The important point to notice is that the risk evaluation could be transferred in a probability evaluation on the initial condition and parameters space. This will still hold for more complex risk functions even if it will be necessary to account for the transformation of coordinate in the phase space and, in case of non-Liouville type of problem, of the diffusion of the probability in the phase space.

The contour of S_{end} is defined as the limit surface (∂S_{end}). In conclusion, a limit surface is a hyper-surface discriminating the input space coordinates (initial condition and model parameters) depending on the evolution that the system will have being located either on the left or right side of the limit surface.

The knowledge of the limit surface allows a fast evaluation of risk functions, provides information concerning which uncertainty is mostly relevant to risk increase/decrease, defines safe areas to be explored for parametric operational optimization and risk reduction. Unfortunately the search of a limit surface in terms of computational effort is very expensive.

A brute force approach would be to build an N-dimensional grid on the input space and sample each point. The number of points in the grid would be proportional to the degree of accuracy sought and would hit rather fast a prohibitive number. To avoid such a situation RAVEN uses acceleration schemes based on Surrogate Models (SM) that are used to predict the location of the limit surface so to guide the exploration of the input space. Such a scheme is shown in figure 7 that will be described after the introduction of the Surrogate Models in the next paragraph.

2.4 Models

First in the RAVEN environment a model is considered whatever could be fully characterized by an input and a corresponding output, essentially a mapping. RAVEN does not possess any models per se but implements APIs by which models could be integrated and sampled by the code. Currently these APIs are implemented for RELAP-7, any generic MOOSE [12] based application, and RELAP5-3D. In addition there is an API for writing directly inside the RAVEN framework a set of python methods that can be interpreted as a model of a physical system. The exchange of data between RAVEN and code representing the physical model (from now on the model) could be performed either by software to software or by files. The APIs leaves future developers free in this respect. Currently, if the model would take a long computational time, it is suggested to transfer the information by files since the parallelism could be better deployed on large clusters. A schema of the information flow and the API interface is reported in figure 8 as a general overview of the working flow. An interesting feature of the RAVEN API for external codes is the fact that the syntax by which the external code interface knows how to modify the input file is completely transparent to RAVEN. RAVEN receives from its input file an association with the a probability distribution and a string, it will pass the sampled value along with the string to the external code interface and will let the interface to interpret the syntax that the developer has chosen for the interface of its specific external code.

2.5 Surrogate Models

In literature there are several definition for surrogate models and/or reduced order models and/or supervised learning process and they sometimes overlap. For the purpose of this article, a surrogate model is a mathematical model that could be trained to predict the response of a physical system. The training is a process that uses sampling of the physical model to improve the prediction capability (capability to predict the status of the system given a realization of the input space) of the surrogate model. More specifically in our case the surrogate model is trained to emulate a numerical representation of the physical system that we assume is performed with a high degree of fidelity but is also very computational expensive to realize. Two general characteristics of surrogate models will be assumed true in the remaining of this discussion even though exceptions are possible:

1. The higher the number of realizations in the training sets the higher the accuracy of the prediction of the surrogate model. This is assumed true although some of the surrogate models used might be

subject to the over-fitting issue. Since this a phenomena that is highly dependent on the surrogate model type it will not be discussed here, given the large number of options available in the RAVEN code. Depending on the cases the user should consult the specific literature on this subject.

2. The smaller the size of the input domain with respect the variability of the system response projected on the cost function, or vice versa, the smoother the response of the system projected on the cost function within the input domain, the more likely the surrogate model will be able to represent the risk function.

Given the fact that most of the time the cost function assume the form of a characteristic function of a certain domain in the phase space, in the development of the RAVEN code it has been given priority to the introduction of a class of supervised learning algorithms that are usually referred to as a classifier. In essence, a classifier is a surrogate model that is capable to represent a binary response of the system (failure/success). In these cases the response that is emulated is therefore $\theta_f(\mathbf{H}(\bar{\mathbf{x}}_0, \bar{\mathbf{p}}, t_{end}) = \bar{\mathbf{x}}(t_{end}))$ as a function of $(\bar{\mathbf{x}}_0, \bar{\mathbf{p}})$.

The first class of classifier introduced has been the Support Vector Machines with several different kernels (polynomial of arbitrary integer order, radial basis function kernel, sigmoid) followed by a nearest-neighbor based classification using a K-D tree search algorithm. All these supervised learning algorithms have been imported via an Application Programming Interfaces (APIs) from the scikit-learn [13] library. It is planned to import the whole library of supervised learning methods from scikit-learn. Also the N-Dimensional spline and the inverse weight methods, that are currently available for the interpolation of N-Dimensional PDF/CDF, will soon be available as surrogate models.

Now it is possible to fully understand the calculation flow in figure 7 where $SM(\bar{\mathbf{x}}_0, \bar{\mathbf{p}}, t_{end})$ indicate the prediction by the SM of $\theta_f(\mathbf{H}(\bar{\mathbf{x}}_0, \bar{\mathbf{p}}, t_{end}))$. Something that has not been yet mentioned is the fact that the point to be sampled next during the iterative algorithm is chosen as the one located in the assumed limit surface that is the most far away from any other already sampled location.

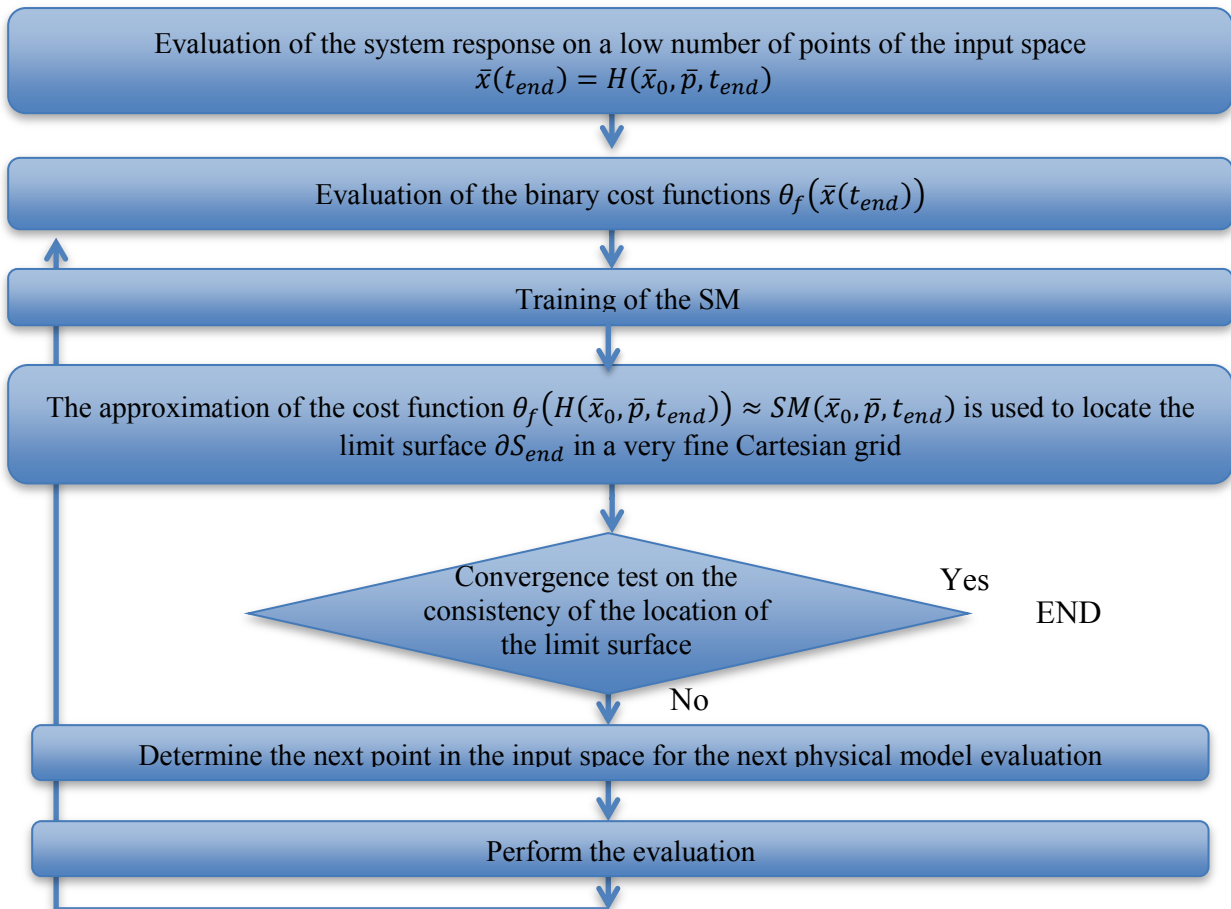


Figure 6: Adaptive limit surface iterative process.

2.6 The Simulation Environment

RAVEN, during a work session, is perceived by the user as a pool of tools and data. Any action in which the tools are applied to the data is considered a ‘step’ in the RAVEN environment. For the scope of the paper we can focus on the multiRun type of step, since all the other are either closely related (single run and adaptive run) or just used to perform data management and visualization. First of all the RAVEN input file associates the variable definition syntax to a set of PDF and to a sampling strategy. As this name says, the multiRun step is used to perform several runs (sampling) in a block of a model, like for example in a Monte Carlo sampling strategy. At the beginning of each sub sequential run of the model the sampler provides the new values of the variables to be modified. The code API places those values properly in the input file. At this point the code API generates the run command and asks to be queued by the job scheduler. The job scheduler handles the parallel execution of as many run as possible within a user prescribed range and communicates with the step controller when a new set of output files are ready to be read. The code API receives the new input files and collects the data in the RAVEN internal format. The sampler is queried to assess if the sequence of runs is ended, if not, the step controller will ask a new set of values from the sampler and the sequence is restarted described in figure

The job scheduler currently is capable to run different run instances of the code in parallel and can also handle codes that are multi threaded underneath or using any form of MPI parallel implementation. RAVEN has also the capability to plot the simulation outcomes while the set of sampling is performed and to store the data for later recovery.

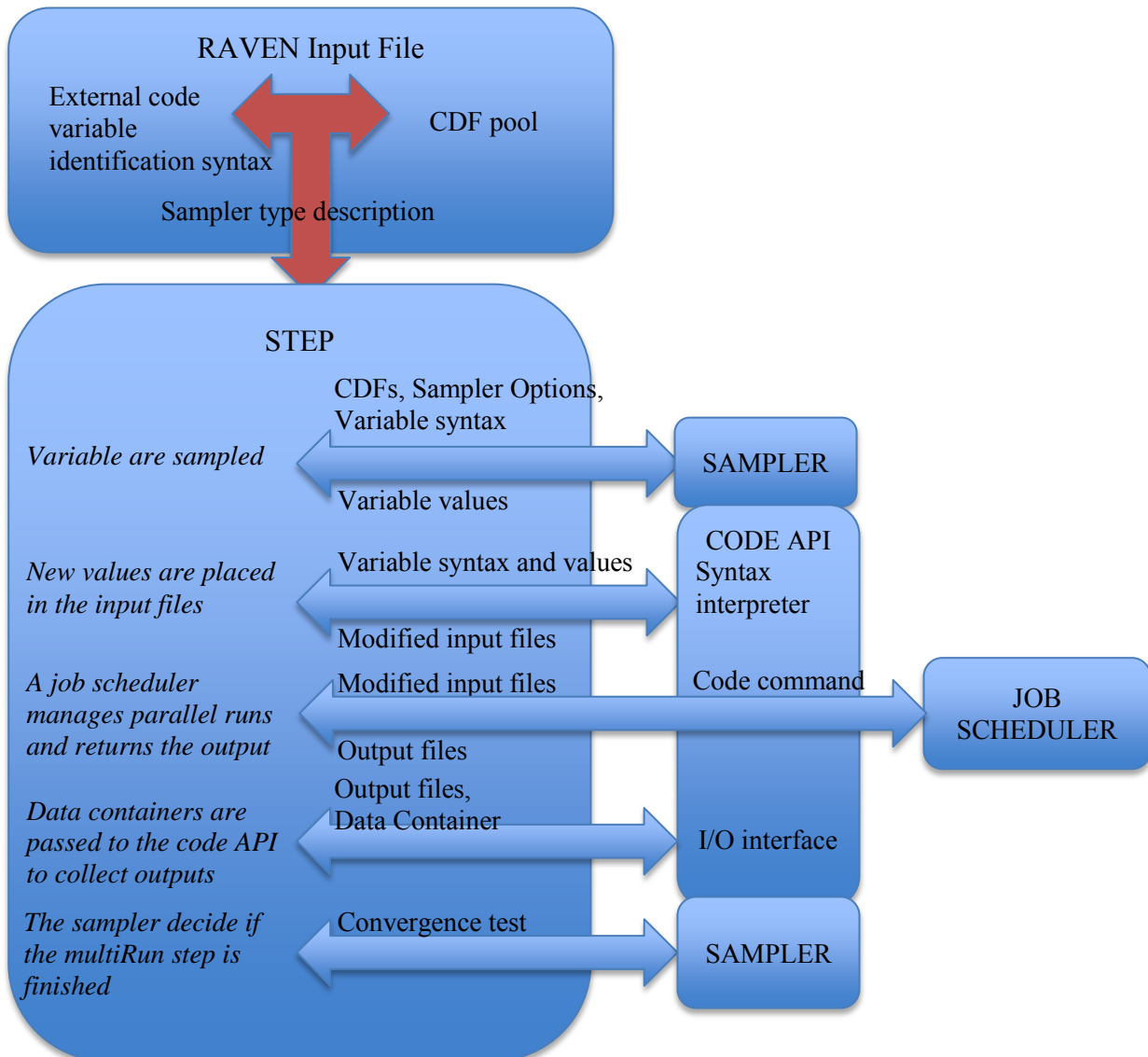


Figure 7: Workflow for the execution of a multi run type of simulation step.

3. EXAMPLES

This section will present some of the results obtained with RAVEN. The focus of this section will be about how the capabilities of RAVEN could be used to perform PRA type of analysis.

3.1 The Reference Case

The case hereafter shortly described will be used overall as a baseline for further exemplification of RAVEN capabilities in addition to few more specialized cases that will be described time by time.

The case is a simplified PWR simulated by RELAP-7 during a Station Black Out condition. Figure 8 shows a visualization of the plant.

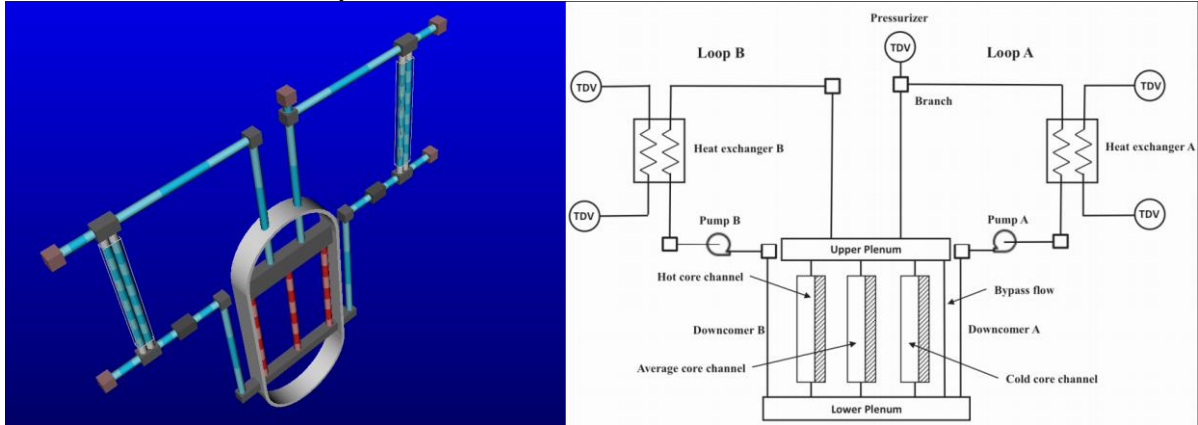


Figure 8: PWR demo plant layout.

3.1.1 The Monte Carlo Analysis

Once that the plant is in SBO condition the probability of recovering the emergency cooling system is set dependent from the recovery of any of the following system:

- Diesel Generators (DGs): the power is restored when two of the three DG train is recovered
 - The recovery time of the first train t_{DG1} is distributed as it follows:

$$\left\{ \begin{array}{l} pdf(t_{DG1}) = Normal(t_{DG1}; \sigma = 200, \mu = 800) \\ 0 < t_{DG1} < 2500 \end{array} \right.$$

- The recovery time of the second train T_{DG2} is distributed as it follows:

$$pdf(t_{DG2}) = pdf(t_{DG2}) * U(x; min = 0.5, max = 1)$$

- Reserve Station Service Transformer recovery time (T_{RSST}):

$$\left\{ \begin{array}{l} pdf(t_{RSST}) = Normal(t_{RSST}; \sigma = 500, \mu = 1400) \\ 0 < t_{DG1} < 2500 \end{array} \right.$$

- The recovery of the main AC line t_{138} is distributed following: $pdf(t_{138}) = Normal(t_{138}; \sigma = 500, \mu = 2000)$

The simulation scope is to assess the failure success of the plant. The goal function associated is:

$$\theta_f(T_{c MAX}, t) = \delta(t - t_{fc})$$

Where $T_{c MAX}$ is the maximum clad temperature and the T_{fc} is the clad failure temperature.

The failure temperature of the clad is also a stochastic variable with triangular distribution:

$$pdf(T_{fc}) = \begin{cases} 0 & \text{if } T_{fc} < 1800F \\ 1 & \text{if } T_{fc} > 2600F \\ 1800 + \frac{0.0025}{400} T_{fc} & \text{if } 1800 < T_{fc} < 2200 \\ 2600 - \frac{0.0025}{400} T_{fc} & \text{if } 2200 < T_{fc} < 2600 \end{cases}$$

Note that the time at which both diesel generators are available needs to be treated as a multidimensional distribution function unless the recovery of the second train is computed inside the system control logic once the recovery time of the first train is already known.

For this analysis, 4000 samples using a Monte Carlo scheme were performed using a batch size of 400 cores on the Fission HPC cluster at the Idaho National Laboratory. In figure 9 it is shown the histograms of the max temperature achieved during the simulation and the clad failure temperature. Failures might happen in the overlapping regions of the histograms, a more detailed discussion on the reading of this plot is reported in [11].

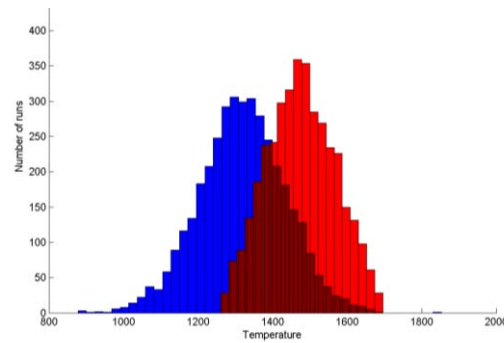


Figure 9: Histogram of the max clad temperature and failure temperature.

3.1.2 The Dynamic Event Tree Analyses

The situation considered is exactly the one presented in the Monte Carlo analysis (3.1.2)1) and the details of the analysis can be found in [11]. Figure 9 shows the time evolution of the clad temperature and a projection of the sampling grid pattern generated by the dynamic event trees approach. The green lines are the simulation continuing while the red dots signal a point where a simulation was stopped since reaching the maximum clad temperature. It could be noticed that there are simulation being stopped at a level of temperature that are exceeded by other simulations. The reason is of course the random value of the clad failure temperature. On the left the plot shows a projection of the threshold triggered by the Dynamic Event Tree simulation of the transient. The projection is performed by defining the recovery time of the auxiliary system $t_{AC} = \min(t_{DG2}, t_{138}, t_{RSST})$. It is clear how the competing variable (max clad temperature and AC recovery time) are alternatively moved towards higher values of their CDF until a transition point between success failure is reached. This pattern is generated by the contemporaneously sampling of two antagonist variables or in a terminology more familiar in the RISMC framework by contemporaneously sampling the capacity and the load. This aspect is discussed more in detail in [11].

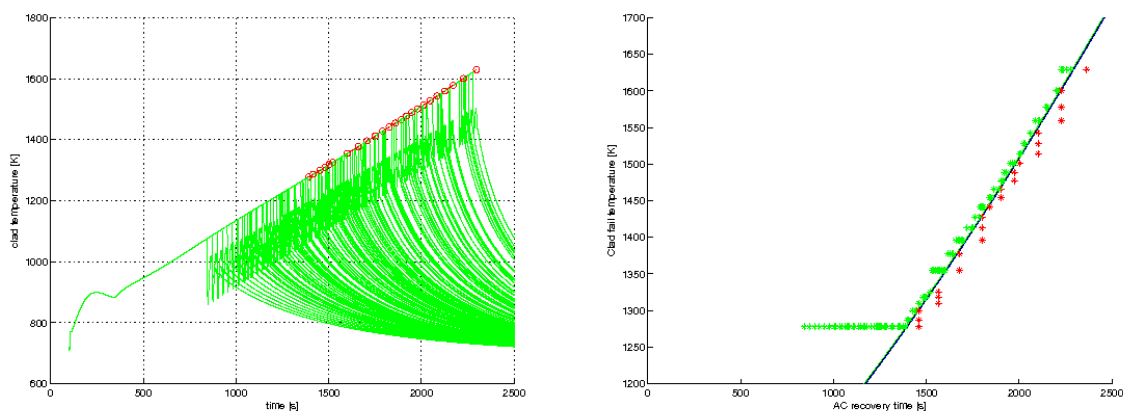


Figure 9: On the left the max clad temperature for each of the branches generated by the dynamic event tree. On the right the point sampled by the dynamic event tree.

3.1.3 Limit Surface Analysis

Figure 10, which is generated of the Monte Carlo Sampling in 3.1.1 shows clearly how (for a fixed value of clad failure temperature) the limit surface is composed by three orthogonal planes. This is clearly due to the fact that in essence the regions of possible system failure the max temperature in the clad could be described by a linear relationship with the recovery time of the auxiliary system. The success condition is therefore:

$$t_{fc} > t_c = t_0 + \alpha \cdot \min(t_{DG2}, t_{138}, t_{RSST})$$

Since the limit surface search algorithms are still in a testing phase rather than the case described in 3.1.1 to illustrate their capabilities it was decided for a simpler case. With the help of the API for the implementation of an external model, as described in 2.4, it was constructed a model returning:

$$t_c = t_0 + \alpha \cdot \min(t_{DG2}, t_{RSST})$$

The model of course was not accurate in terms of numbers but it was supposed to show a similar behavior even if one of the sampled recovery times was suppressed to allow a 3D visualization of the limit surface for varying failure temperature of the clad.

Figure 10 shows the two limit surfaces obtained with a nearest neighbor (on the right) and radial basis function (RBF) based surrogate models. Both limit surface show the two bounding planes compared to the safe space (side of the surface with low recovery times) increase with the raising of the failure temperature of the clad. This is clearly observable by the inclination of the planes. The nearest neighbor as expected presents sharper edges with respect to the RBF kernel that instead tends to soften the borders. The nearest neighbor algorithm closed the top of the surface erroneously; this unexpected behavior is still under investigation.

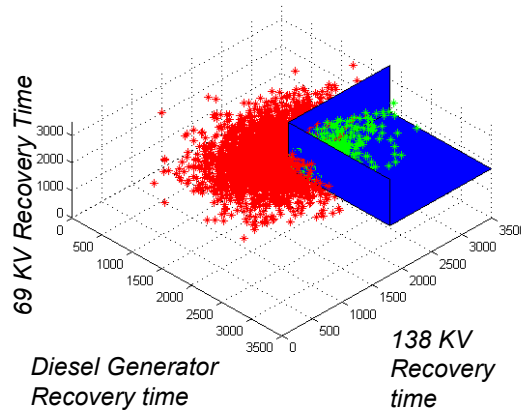


Figure 10: Classification of the input space for the PWR SBO depending if during the simulation the max clad temperature has been (failure, green), or have not been (success red) exceeded. To obtain a 3D plot the T_{fc} has been kept constant at 1477 K.

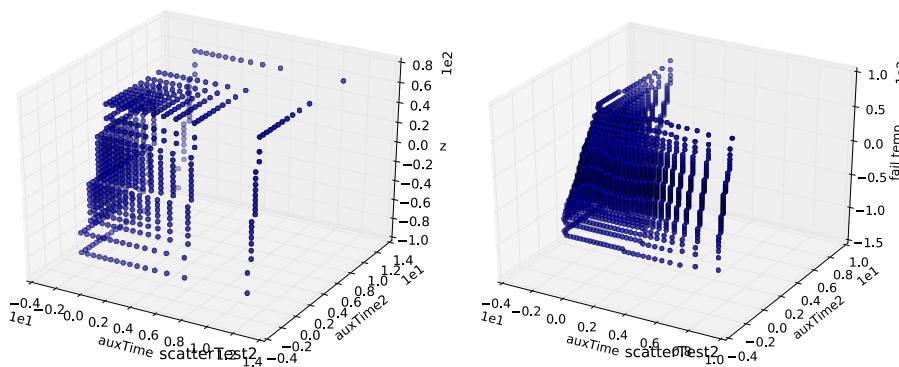


Figure 11: On the left the max clad temperature for each of the branches generated by the dynamic

4. CONCLUSION

RAVEN is reaching a level of maturity that might lead soon to a release of the code outside Idaho National Laboratory to collect the first feedback. The statistical analysis framework based on grids and

Monte Carlo relies on very well assessed methodologies, and seems solid already. The integration of those methodologies with the data handling flexibility, the visualization capabilities (all plots are directly generated by the RAVEN code) and the ease of coupling with different physical model simulators shows how RAVEN can be a powerful tool for PRA analysis. The dynamic event tree implementation allows also a rapid turnaround time for the coupling with other codes as long as access to the simulator of control logic is provided. The dynamic event trees has been identified as one of the most promising approaches for PRA and at the same time it is foreseen its additional development to introduce adaptivity.

Moreover the coming release of the code will the familiarize the PRA community with this enhanced techniques like limit surface or surrogate model construction for identifying the leading mechanisms of the system failure.

Acknowledgements

This work is supported by the U.S. Department of Energy, under DOE Idaho Operations Office Contract DE-AC07-05ID14517. Accordingly, the U.S. Government retains a nonexclusive, royalty-free license to publish or reproduce the published form of this contribution, or allow others to do so, for U.S. Government purposes.

References

- [1] D. Anders, R. Berry, D. Gaston, R. Martineau, J. Peterson, H. Zhang, H. Zhao, and L. Zou, "Relap-7 level 2 milestone report: Demonstration of a steady state single phase pwr simulation with relap-7," Tech. Rep. INL/EXT-12-25924, Idaho National Laboratory (INL), 2012.
- [2] C. Rabiti, A. Alfonsi, J. Cogliati, D. Mandelli, and R. Kinoshita, "Reactor analysis and virtual control environment (raven) fy12 report," Tech. Rep. INL/EXT-12-27351, Idaho National Laboratory (INL), 2012.
- [3] C. Rabiti, D. M. A. Alfonsi, J. Cogliati, and B. Kinoshita, "Mathematical framework for the analysis of dynamic stochastic systems with the raven code," in Proceedings of International Conference of mathematics and Computational Methods Applied to Nuclear Science and Engineering (M&C 2013), Sun Valley (Idaho), pp. 320–332, 2013.
- [4] Alfonsi, C. Rabiti, D. Mandelli, J. Cogliati, and B. Kinoshita, "Raven as a tool for dynamic probabilistic risk assessment: Software overview," in Proceedings of International Conference of mathematics and Computational Methods Applied to Nuclear Science and Engineering (M&C 2013), Sun Valley (Idaho), pp. 1247–1261, 2013.
- [5] Smith, C. Rabiti and R. Martineau, "Risk Informed Safety Margins Characterization (RISMC) Pathway Technical Program Plan," INL/EXT-11-22977, November 2012
- [6] RELAP5-3D© Code Manual, Vol.1-5, Rev. 3, INEEL-EXT-98-00834 (2009)
- [7] R.L. Williamson, J.D. Hales, S.R. Novascone, M.R. Tonks, D.R. Gaston, C.J. Permann, D. Andrs, R.C. Martineau, "Multidimensional multiphysics simulation of nuclear fuel behavior", *Journal of Nuclear Materials*, 423 (2012) 149–163
- [8] Boost Team, <http://www.boost.org>
- [9] Christian Habermann, Fabian Kindermann, "Multidimensional Spline Interpolation: Theory and Applications", *Computational Economics*, Volume 30, Issue 2, pp 153-169, 2007
- [10] William J. Gordon and James A. Wixom, "Shepard's Method of "Metric Interpolation" to Bivariate and Multivariate Interpolation", *Mathematics and Computation*, vol. 32, n 141, pp 253-264, 1978.
- [11] Alfonsi, C. Rabiti, D. Mandelli, J. Cogliati, B. Kinoshita, and A. Naviglio. "Dynamic event tree analysis through Raven". In Proceedings of ANS PSA 2013 International Topical Meeting on Probabilistic Safety Assessment and Analysis, Columbia (South Carolina), 2013.
- [12] Gaston, G. Hansen, S. Kadioglu, D. A. Knoll, C. Newman, H. Park, C. Permann, and W. Taitano, "Parallel multiphysics algorithms and software for computational nuclear engineering," *Journal of Physics: Conference Series*, vol. 180, no. 1, p. 012012, 2009.
- [13] Pedregosa et al., "Scikit-learn: Machine Learning in Python", *Journal of Machine Learning Research*, pp. 2825-2830, 2011.